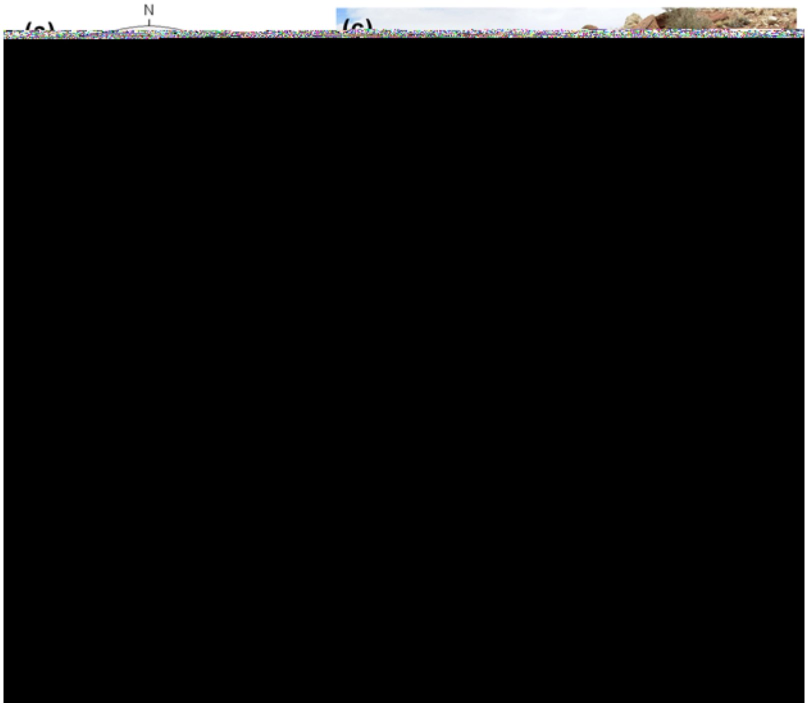

Figure 11. (a and b) Equal-area plots of great circles and pole density contours representing the geometry of the overturned siltstone bed (Moqui Member of the Moenkopi Formation) at the base of the ejecta blanket that exposed on the upper crater wall. The overturned flap appears like a cylindrical fold. (c) A field photograph showing the overturned flap at the location of Figure 11b; look direction is approximately NNW. The geologic map is the same as Figure 2a.

relatively small rim height at Lonar Crater are produced by a combination of the inherent strength of basalt relative to sedimentary rocks and the lack of a preexisting fracture system like that at Meteor Crater. The relative contributions of these two factors, however, still need to be resolved.

7. Fractures in Artificial Craters: Implications for Impact Fracturing

[19] Laboratory experimental impact craters on rocks and ice, plus small-scale impacts on spacecraft components, generate impact fracture networks that may provide insights to impact fracturing [e.g., *Polanskey and Ahrens*, 1990; *Arakawa et al.*, 2000; *Graham et al.*, 2004]. It appears that deformational processes of these strength-controlled artificial craters are similar to those of strength-controlled natural simple craters [*Ahrens et al.*, 2002]. The distribution of impact fractures and their relative ages are shown in a plan view of the images of cratered solar panels (Figures 14a and 14b), which are permeated with concentric fractures and/or damage zones and radial fractures. While the radial fractures predate the concentric zones, in some cases they postdate them. For example, the radial fractures have developed from the concentric damage zones (Figure 14a); in other cases, the concentric zones limit the growth of radial ones (Figure 14b). More interestingly, in some instances, many of the radial fractures appear very similar to the branching-type dynamic tensile fractures produced in laboratory experiments. This points to the growth of very high velocity fractures during the impact [see *Sagy et al.*, 2001]. A vertical section across the laboratory impact crater (Figure 14c) on gabbro reveals the sets of radial and concentric fractures below a zone of near-surface fractures, location of which coincides with the theoretical near-surface zone predicted by a spallation model [*Polanskey and Ahrens*, 1990] (Figure 14c). The relative age relationship between the radial and concentric fractures in vertical section is also the same as those seen on the plan view of spacecraft craters.

[20] The radial and concentric fractures seen on the plan view of Meteor Crater (Figures 6 and 7) appear similar to those of the artificial craters (Figures 14a and 14b), and probably, the conical fractures of the Meteor Crater (Figure 8) are comparable to the radial fractures seen on the vertical section of the artificial crater (Figure 14c). However, it must be remembered that the radial and concentric fractures of Meteor Crater are largely produced by reactivation of preimpact tectonic fractures, and those formed in the artificial craters are purely related to impacts, as the targets of artificial craters do not appear to contain any visible preimpact fracture systems. Therefore, the comparison does not necessarily reflect the same mechanism of fracture formation. It is worth mentioning here that there have been no experimental or numerical studies that describe how impact fractures would form in the presence of closely or regularly spaced preimpact fracture systems in the target rocks. Obviously, preimpact weakness zones would reduce the dynamic strength of the